ACS APPLIED MATERIALS & INTERFACES

Research Article

www.acsami.org

A Novel Approach for the in Situ Synthesis of Pt−Pd Nanoalloys Supported on Fe_3O_4@C Core−Shell Nanoparticles with Enhanced Catalytic Activity for Reduction Reactions

Peng Zhang, Ren Li,* Yimin Huang, and Qianwang Chen*

Hefei National Laboratory for Physical Sciences at Microscale and Department of Materials of Science and Engineering, University of Science and Technology of China, Hefei 230026, China

Supporting Information

ABSTRACT: A facile two-step synthesis method has been developed for the synthesis of highly active and well-defined Pt−Pd nanoalloys supported on the surface of Fe_3O_4@C colloidal nanoparticles. The nanoalloys were characterized by X-ray diffraction (XRD), high-resolution transmission electron microscopy (HRTEM), scanning transmission electron microscopy (STEM) with line scanning of energy-dispersive X-ray spectroscopy (EDS) and X-ray photoelectron spectroscopy. The nanoalloys exhibit remarkable catalytic activity toward reduction of 4-nitrophenol to 4-aminophenol by $NaBH_4$. Furthermore, the catalytic activity of the supported nanoalloys could be further optimized by tuning the composition of the supported nanoalloys, and the optimized catalytic activity is obtained with a normalized rate constant of about 12.03 $nmol^{-1}$ s^{-1} when the atomic ratio of Pd to Pt is tuned to 2.07:1, which is advancing among the Pd-based nanocatalysts reported in the recent years.

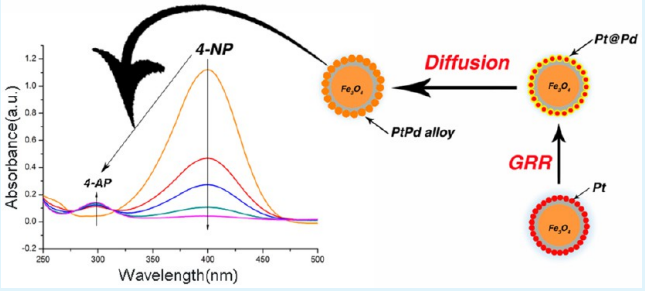

KEYWORDS: *in situ, Pt−Pd nanoalloy, reduction, 4-nitrophenol, catalyst*

1. INTRODUCTION

Bimetallic nanoparticles consisted of two different metal elements have attracted great interests in the field of science and technology because of their wide applications in various fields.[1−3] Particularly, bimetallic nanocatalysts have received intensive study because of their unique properties superior to their monometallic analogues. For instance, we can improve specific physical and chemical properties, especially catalytic properties, by changing the composition of the two metals or their structures from heterostructures to core−shell structures, nanoalloys, intermetallic, etc.[4−7] What's more important is that the performance of bimetallic nanocatalysts could be enhanced, such as selectivity, durability and stability. For example, Bernardotto and co-workers observed that doping Pd with either Pt or Au can improve the selectivity and productivity of H_2O_2 compared with the monometallic samples for the direct synthesis of hydrogen peroxide under very mild conditions.[8] Wang et al. developed a one-step reduction route to synthesize Pd-rich carbon-supported Pd−Pt alloy catalysts, which exhibited more excellent oxygen reduction activity and much higher methanol tolerance than the commercial Pt/C catalyst.[9] More intriguing, in most cases, the bimetallic nanocatalysts show superior activity than the simple mixture of their monometallic counterparts in performance.[10−13] Xia reported a simple galvanic replacement approach to the synthesis of Pt−Pd bimetallic nanoparticles on carbon black with an extremely high activity toward formic acid electrooxidation, and the catalytic activity of Pt-decorated Pd/C was 143 times high than that of Pt/C and 5 times higher than that of Pd/C, respectively.[14] Hence the bimetallic catalysts found applications in the widespread field such as chemical industry and energy science.[15,16]

Although the bimetallic catalysts dispaly outstanding properties, it is often the case that a sudden drop in catalytic activities is experienced after the catalytic transformation on account of the aggregation and leaching of the bimetallic catalysts. Hence, a number of efforts have been devoted to develop feasible routes for immobilizing or grafting the bimetallic catalysts onto inorganic supports to improve their stabilization and recycling stability. Typically, Li et al. reported a simple physical deposition approach to prepare Pt−Pd hybrid catalysts supported on a nitrogen-modified carbon composite, and the hybrid catalysts possessed highly stability for oxygen reduction reaction.[17] Jiang et al. stabilized bimetallic Au@Ag core−shell nanoparticles on a metal-organic framework, which makes for the excellent recyclable performance.[18] In general, supported bimetallic catalysts are achieved by means of conventional impregnation methods,[19,20] mostly by anchoring or physically adsorbing the bimetallic nanoparticles previously prepared on a functionalized support,[21,22] which would be different from the

Received: November 18, 2013
Accepted: February 4, 2014
Published: February 4, 2014

ACS Publications © 2014 American Chemical Society

dx.doi.org/10.1021/am405167h | ACS Appl. Mater. Interfaces 2014, 6, 2671−2678

Scheme 1. Schematic of Synthetic Procedure of Fe_3O_4@C@PtPd Hybrid Nanoparticles

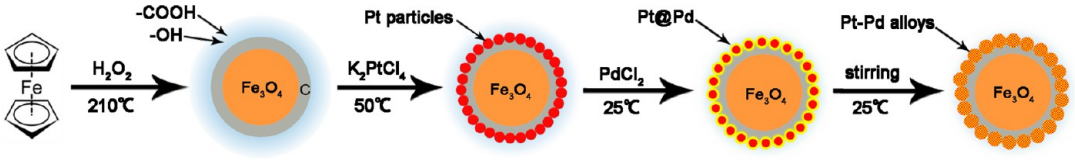

supported monometallic nanoparticles that could generate in situ easily. As far as we know, an in situ route is beneficial to promote activity of the supported metallic nanocatalysts owing to a change in the electron properties of active sites of the metal by electron transfer between metallic nanocatalysts and supports or, more succinctly, a synergetic effect coming up between them.[23,24] What is more, surface detachment for the bimetallic nanoparticles can be avoided because of its strong adhesion with the supports generated by an in situ synthesis route.

Because there are only several reports about preparing the supported bimetallic catalysts by an in situ formation method, and to the best of our knowledge, few have succeeded to obtain bimetallic nanocrystals on substrates,[25] most of the results turned out to be monometallic counterparts anchoring on substrates.[26−28] So it still remains a grand challenge to in situ generate well-defined bimetallic nanoparticles on a support. This work aims to develop a facile way for in situ growth of the bimetallic nanocrystals on substrates. The different supports could give rise to different effects on the catalytic properties.[29−31] Hence, searching for a desirable support is crucial to improve the catalytic properties of nanocatalysts as well. In our present research, the carbon-encapsulated superparamagnetic colloidal nanoparticles (CMNPs) that were fabricated via a one-step solvothermal process were used for catalyst supports based on our previous work.[32] This is an excellent support in virtue of high monodispersity, enhanced stability at high temperature, high saturation magnetization, high negative charges, and good dispersibility in the aqueous solution in favor of catalytic liquid-phase reaction, which has been affirmed by our earlier work.[33,34]

The colloidal metal alloy nanoparticles, especially platinum and palladium alloys have been the outstanding choice of catalysts in many important chemical and electrochemical reactions.[7,17,35−37] It is well known that co-reduction is the most common preparative method of bimetallic nanoalloys. However, it is difficult to control the reduction and nucleation of two different types of metals simultaneously, resulting in the separation of nucleated monometallic Pd and Pt particles and worse than that, utilization of supports exacerbates the deficiency in the process of co-reduction because of the difference of their redox potential and chemical properties.[16,38,39] Consequently, it is difficult to generate supported nanoalloys in situ. Here, we report a method to prepare Pd−Pt alloy nanoaprticles by the atomic diffusion between bimetallic platinum and palladium as shown in Scheme 1. Firstly, Pt nanoparticles were deposited on the surface of the supports by the alcohol reduction, and then we take advantage of galvanic replacement reaction (GRR) and rapid inter-diffusion of Pt and Pd atoms in the reduced dimension of nanoparticles. Pd atoms in situ form on the surface of Pt nanoparticles and diffuse into the Pt nanoparticles at room temperature, which finally brings about the formation of the Pt−Pd nanoalloys on the surface of supports. It was found that the as-prepared Fe_3O_4@C@PtPd hybrid nanoparticles exhibit an ultrahigh activity as catalysts for the reduction of 4-nitrophenol (4-NP) to 4-aminophenol (4-AP) by $NaBH_4$.

2. EXPERIMENTAL SECTION

2.1. Materials. Ferrocene ($Fe(C_5H_5)_2$,≥98%), hydrogen peroxide (H_2O_2,30%), and acetone (C_3H_6O,≥99%), potassium tetrachloroplatinate (K_2PtCl_4≥96%), palladium chloride ($PdCl_2$, ≥98.4%), sodium borohydride ($NaBH_4$,≥96%), and 4-nitrophenol (99%, analytic grade) were bought analytic grade from the Shanghai Chemical Factory, China. All chemicals were used as received without further purification. Deionized water of resistivity greater than 17.0 MΩ cm was used in all experiments.

2.2. Preparation of Fe_3O_4@C@Pt Samples (simplified as S_{Pt}). Pt nanocrystals were deposited on the CMNPs according to the ethanol reducing method. The carboxyl functionalized Fe_3O_4@C colloidal nanoparticles with diameters of 150 nm were obtained according to our previous reported method.[40] The purified Fe_3O_4@C colloidal nanoparticles were dispersed in ethanol to form the colloidal solution with a concentration of about 3 mg/mL. Then 1 mL of the colloidal solution was added into ethanol and deionized water mixture solution (1:1, v:v) with mechanical stirring, followed by adding dropwise 0.3 mL of 0.01 mol/L K_2PtCl_4 at room temperature and kept stirring for 30 min. Then, the mixed solution was incubated at 50 °C for 3 h. After that, the product was centrifuged (7500 rpm, 5 min) and washed at least four times with deionized water. Finally, the purified product was dispersed in 30 mL of deionized water for further use.

2.3. Preparation of Fe_3O_4@C@PtPd Nanocatalysts. Fe_3O_4@C@PtPd nanocatalysts were prepared by a facile method based on the GRR to facilitate the growth of reduced Pd atoms on Pt nanocrystals. In a typical process, 0.263 mL of aqueous solution of $PdCl_2$ (5.71 mmol/L) was added into 30 mL of Fe_3O_4@C@Pt in an aqueous solution with mechanical stirring at room temperature for 8 h. The final products were washed several times with deionized water and ethanol and dried in a vacuum oven.

2.4. Catalytic Reaction of Reduction of 4-NP. The reaction proceeded under ambient conditions. Typically, 0.1 mL of aqueous solution of 4-NP (0.03M), 2.4 mL of deionized water, and 0.4 mL of aqueous solution of a fresh $NaBH_4$ (0.3M) were added into a quartz cuvette, and then adding 100 μL of aqueous solution of Fe_3O_4@C@PtPd nanocatalysts (the nanocatalysts were dispersed in 5 mL of deionized water). The change of the mixture solution color was monitored using UV−vis spectroscopy, and the decrease in absorbance at 400 nm was recorded at 0.5 s intervals by time scanning of the UV spectrometer.

2.5. Characterization. The powder X-ray diffraction patterns were collected on a X-ray diffractometer (Japan Rigaku D/MAX-γA) equipped with Cu Kα radiation (λ = 1.54178 Å) over the 2θ range of 30−90°. The morphologies of all samples were viewed using a transmission electron microscope (TEM, Hitachi model H-800). The Pd and Pt content of samples were analyzed by means of an inductively coupled plasma (ICP) spectrometer (Optima 7300 DV). The distribution of element of the magnetic hybrid nanoparticles was characterized using the atomic resolution analytical transmission electron microscopy (ARTEM, JEM-ARM200F) with energy dispersive X-ray (EDS, Oxford). X-ray Photoelectron Spectroscopy was carried out on an ESCALAB-250 spectrometer (Thermo Corp.) equipped with an Al Kα X-ray exciting source (1486.6 eV) operated at 195 W with a 14.8 kV acceleration voltage. The UV−vis absorption spectra were recorded on a UV−vis spectrophotometer (TU-1810, Beijing).

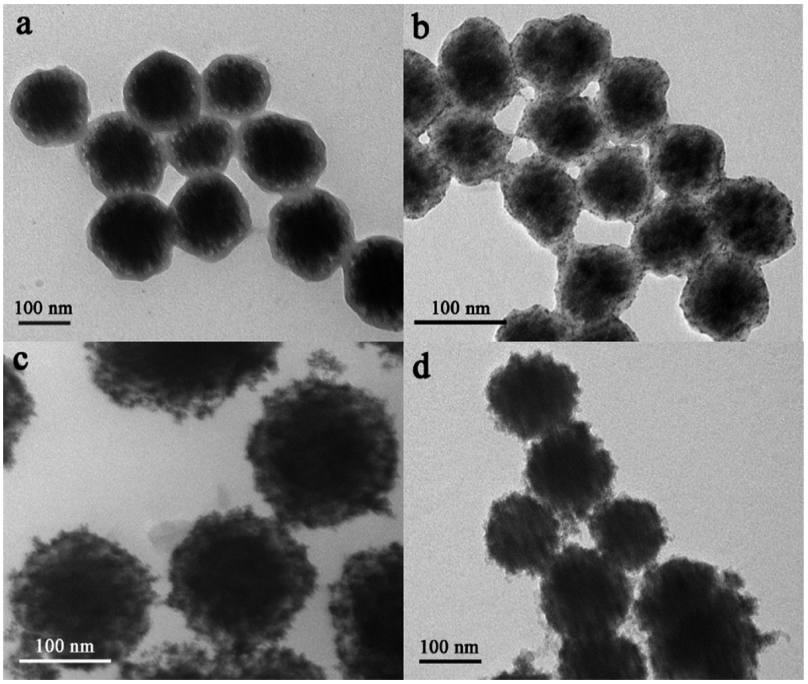

Figure 1. TEM images of the (a) CMNPs, (b, c) Fe_3O_4@C@Pt nanoparticles, and (d) Fe_3O_4@C@PtPd nanocomposites corresponding to c.

3. RESULTS AND DISCUSSION

3.1. Characterization of Defined Pt−Pd Nanoalloys on Fe_3O_4@C Colloidal Nanoparticles. The Fe_3O_4@C colloidal nanoparticles, namely the supports, were synthesized via a one-step solvothermal process with a mean diameter of ∼150 nm and the carbon shell is about 15 nm thick as shown in Figure 1a. The carbon shells provide continuous coverage for superparamagnetic Fe_3O_4 nanoclusters and promote the stability of Fe_3O_4 nanoclusters.

The first step of the synthesis route is in situ generation of Pt nanoparticles on the surface of CMNPs via alcohol reduction of K_2PtCl_4. Most platinum precursors can be adsorbed and reduced in situ on the CMNPs because CMNPs have numerous surface functional groups such as carboxyl and hydroxyl moieties. This surface properties of the CMNPs are suitable for catalyst fabrication by avoiding a process of cumbersome surface functionalization and making the surface of the as-prepared nanocatalysts clean. Images b and c in Figure 1 showed that we could easily control the coverage of Pt nanoparticles on the surface of CMNPs by varying the temperature of the experiments in the first step. When the reaction was performed at 45°C, Pt nanodots were deposited on the surface of CMNPs, which results in the formation of core−satellite structures (Figure 1b). When the temperature increases to 50°C, large amounts of Pt nanoparticles with approximate sizes of 10−20 nm were deposited on the surface of the carbon shells, as is shown in Figure 1c.

In the second step, the Fe_3O_4@C@PtPd nanoparticles, shown in Figure 1d, were prepared based on the samples shown in Figure 1c through a GRR, which shows a remarkably simple method to the preparation of bimetallic nanoparticles with versatile structures.[41−43] From Figure 1d, we found the coverage of bimetallic nanoparticles on the supports has a higher density than that of monometallic nanoparticles Pt on the same supports which can be observed more clearly in Figure S1 in the Supporting Information, while the dispersibility of Fe_3O_4@C@PtPd nanoparticles remains unchanged. No agglomeration was observed, which is essential for catalysis. In the following step, it is feasible to achieve galvanic replacement between $PdCl_2$ and Pt nanocrystals in the presence of the supports since the standard reduction potential of Pd^{2+}/Pd (0.915 V) is higher than that of $PtCl_4^{2-}$/Pt (0.758 V),[44] as a result, Pd atoms can replace the Pt atoms on the surface of Pt. Before GRR process, the solution of prepared Fe_3O_4@C@Pt must be changed to pure aqueous solution, otherwise the palladium precursors would be reduced by ethanol before the galvanic replacement reaction proceeds at room temperature, which will lead to deposition of Pd on the surface of the supports rather than Pt nanoparticles. It is found that the reduction of the precursors of noble metals by ethanol occurs easily on the surface of CMNPs support at room temperature according to our experiments, such as Au, Pd, Pt, and even Ag precursor, whereas the precursor of Ag can only be reduced by ethanol as temperature rises over 80 °C.[45] It is suggested that the chemisorption of noble metal ions on the supports increases the reduction potential of them.

Powder X-ray diffraction (PXRD) is used to differentiate alloys from core/shell structure.[46] Figure S2 in the Supporting Information shows the typical XRD patterns for as-synthesized the CMNPs, Fe_3O_4@C@Pt and Fe_3O_4@C@PtPd nanocomposites. The characteristic diffraction peaks of obtained CMNPs could all be indexed to the cubic structure of Fe_3O_4 (JCPDS No.19-0629), indicating the existence of magnetic components in the as-synthesized products. The diffraction pattern of Fe_3O_4@C@Pt samples exhibits peaks at 2θ = 39.9, 46.4, 68.1, and 81.5°, corresponding to the (111), (200), (220), and (311) plane of face centered cubic (fcc) Pt (JCPDS No.01−1190). The XRD pattern of Fe_3O_4@C@PtPd samples, similar to that of Fe_3O_4@C@Pt samples with slight shifts to higher degrees in peak positions, implyed the formation of the structure Pt−Pd alloy are fcc phase. We attribute it to the fact that Pd and Pt share the same face-centered cubic crystal structure and have almost equal lattice constant (with a mismatch of only 0.77%), which facilitates the rapid

interdiffusion of Pd and Pt atoms in the reduced dimension of nanoparticles, and makes the as-obtained Pt−Pd alloys remain are still fcc crystal structure with no significant lattice contraction. As a minor lattice mismatch of only 0.77% cannot be resolved by our diffractometer, extra experiments are needed to ascertain the structure of the Pt−Pd bimetals.

Images a and b in Figure 2 present HRTEM images of the supported Pt−Pd nanoalloys, clearly displaying the distribution

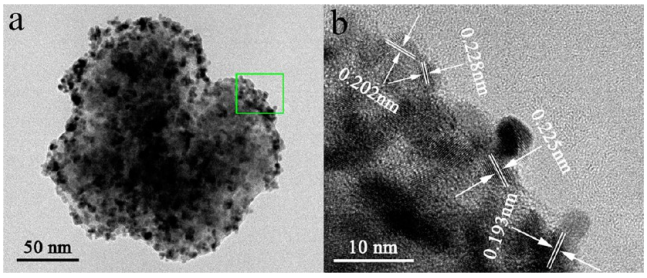

Figure 2. (a) HRTEM image of Fe_3O_4@C@PtPd nanocomposites; (b) lattice fringe of Pt−Pd nanoalloys is the magnified image of the interface enclosed by the green rectangular area in a.

of Pt−Pd nanoalloys on the supports. The estimated lattice spacing of 0.202 and 0.193 nm can be assigned to the (200) planes of Pt−Pd bimetallic nanocrystals and 0.228 and 0.225 nm to (111) planes. This looks similar to the lattice spacing of Pt crystals (200) plane indexed to 0.196 nm and (111) plane indexed to 0.226 nm, and it is noted that the relative error in the estimated result of lattice spacing is a little bit higher than the lattice mismatch between Pt and Pd crystals, therefore, the phase and structure of the as-prepared samples can not be determined only on the basis of HRTEM analysis.

As shown in panels b and e in Figure 3, the EDS results of line scan analysis unambiguously demonstrate the alloy structure of Pt−Pd bimetallic nanocrystals. It can be seen clearly that the Pt−Pd nanocrystals show single Gaussian distributions of X-rays across the particles for both elements. Both elements are uniformly distributed in the nanocrystals, revealing that the nanocrystals have an alloy structure. It proves that Pd atoms on the surface of Pt nanoparticles diffuse into Pt nanoparticles at room temperature when Pd atoms replace Pt atoms and deposite on the surface of Pt nanoparticles by taking advantage of GRR.

The Fe_3O_4@C@PtPd samples with a Pt−Pd molar ratio of 2:1 (labeled as L_1) in Figure 3a have been prepared for 8 h in the second step. When we decreased the reaction time to 0.5 h, the Pt−Pd the molar ratio was changed to 4:1, the structure of as-obtained Pt−Pd nanocrystals (labeled as L_2) is still alloy as illustrated in Figure 3e. The survey of the two samples with different composition of Pd−Pt indicates Pd atoms diffuse into Pt nanoparticles, while Pd atoms take place of surface atoms of Pt nanoparticles through GRR. The more interesting circumstance is that the GRR and diffusion all proceed at room temperature. In general, atomic diffusion comes up under favored reaction conditions such as high temperatures in order to get over the critical energy barrier,[37] although the formation of alloy is usually thermodynamically favored.[47] For instance, Sun and Zhang independently prepared Ag−Au alloy nanoparticles by a replacement reaction and inter-diffusion at 100 °C.[48,49] The room temperature formation could be attributed to the relative small size of Pt nanocrystals (around 5 nm) and an identical crystal structure between Pt and Pd elements with a minor lattice mismatch. The corresponding EDS results of two samples are also shown in panels c and f in Figure 3, where EDS shows the existence of Pt and Pd elements in samples L_1 and L_2 with an atomic ratio of 68:32 and 71:29, respectively. This is equivalent to approximately 32 and 29% of Pt nanoparticles being replaced by Pd-based particles on the basis of the fact that one Pd atom is formed for every one Pt atom consumed, according to the stoichiometry of the replacement reaction when metallic Pt reacts with precursors of Pd.

The surface chemical state and composition of Fe_3O_4@C@PtPd nanocomposites were obtained by XPS in comparison with CMNPs and Fe_3O_4@C@Pt nanoparticles. From the XPS survey scan spectra in Figure S3 in the Supporting Information, the XPS peaks of Pd3d, Pt4f, C1s and O1s can be found for the supported Pt/Pd nanoalloys, confirming the presence of Pt and

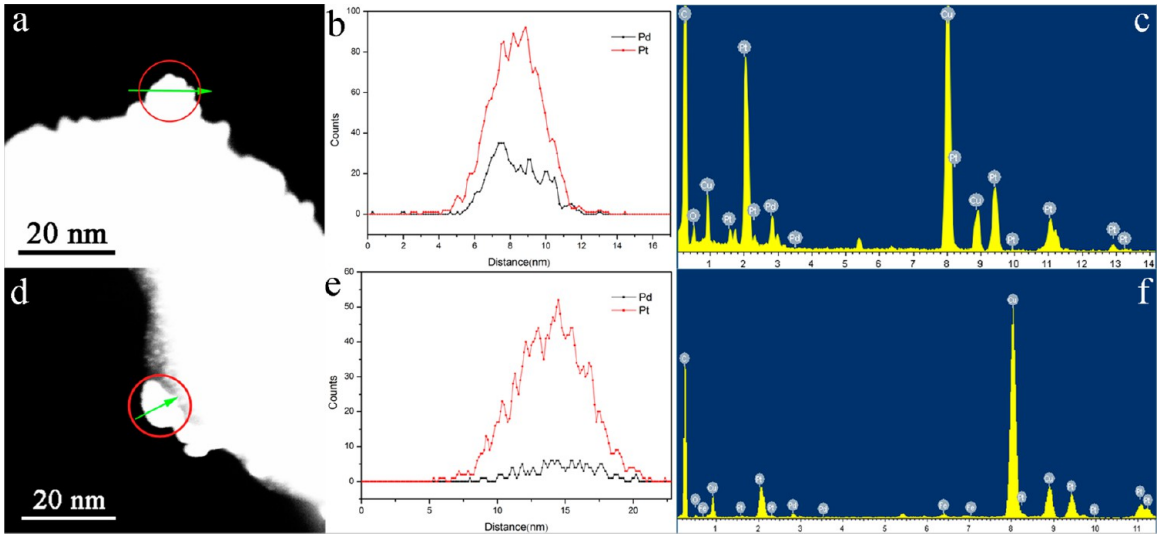

Figure 3. (b, e) EDS line-scanning profile for Pt (red line) and Pd (black line) concentrations in Pt−Pd nanoalloys of (a) and (d) at different ratio of Pt to Pd. Direction of the line scan is indicated with a green arrow, and the red circular region of panels a and d provide the EDS corresponding to (c) and (f).

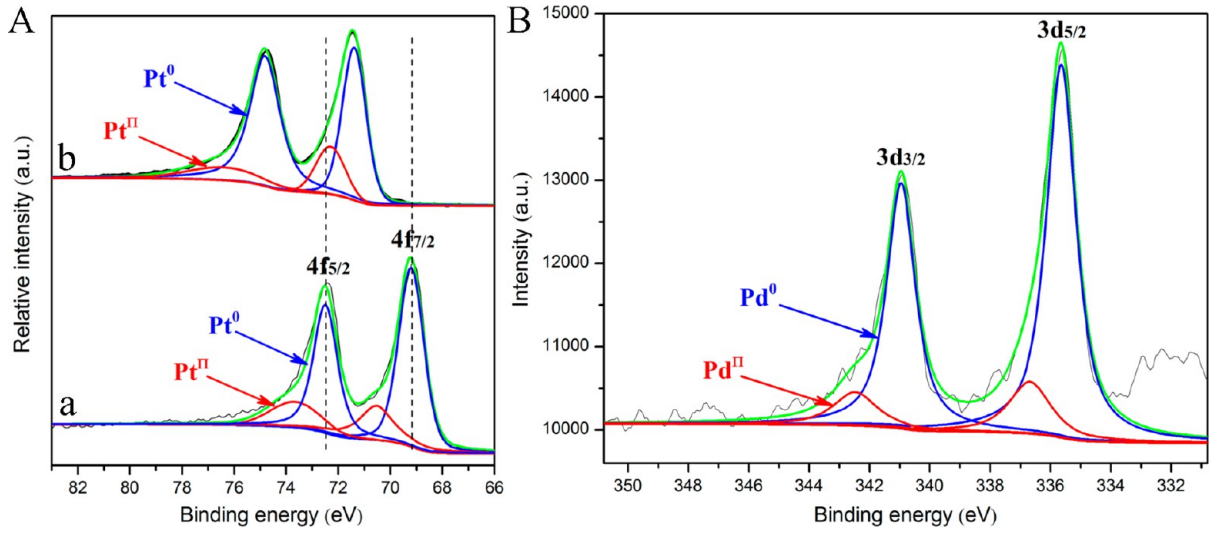

Figure 4. (A) Pt4f XPS spectra of (a) Fe_3O_4@C@Pt and (b) Fe_3O_4@C@PtPd nanocomposites. (B) XPS spectrum of Fe_3O_4@C@PtPd nanocomposites in the Pd3d region.

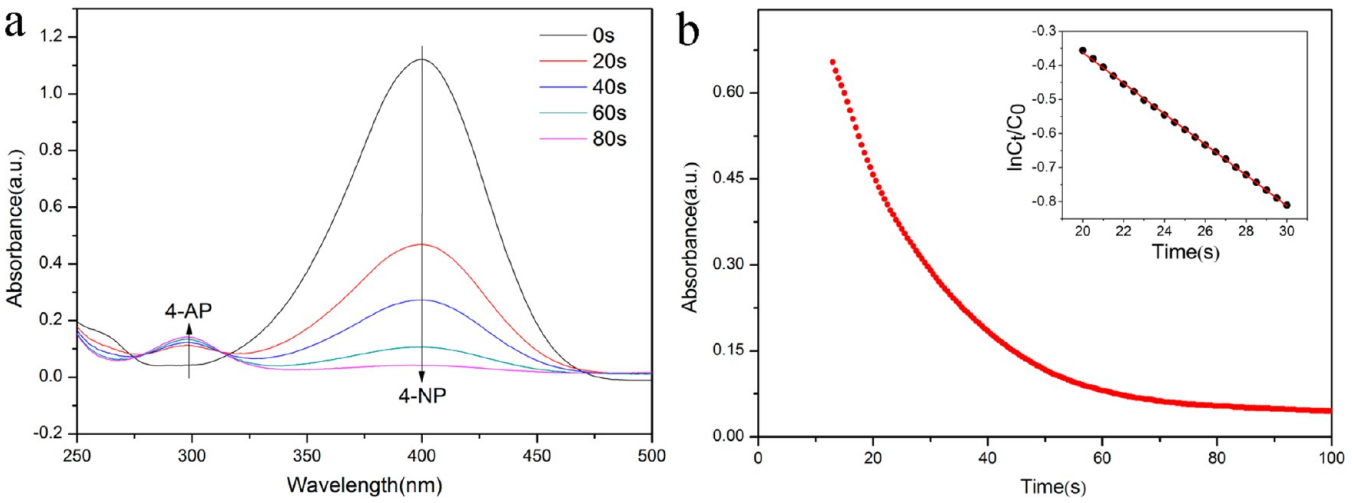

Figure 5. (a) Variation in UV−visible absorption spectra at 20 s intervals for the 4-NP reduction reaction in the presence of Fe_3O_4@C@PtPd nanocomposites. (b) Time dependence of the absorption of p-NP at 400 nm. ([4-NP] = 5.0×10^{-5} mol/L; [$NaBH_4$] = 2.0×10^{-3} mol/L; [PtPd] = 18×10^{-6} mol/L).

Pd in Fe_3O_4@Ccolloidal nanoparticles. The Pt 4f signals of Fe_3O_4@C@Pt and Fe_3O_4@C@PtPd nanocomposites are deconvoluted into two double components by Lorentzian-Gaussian line shape fitting in the spectrum of Figure 4A. The binding energies of two pairs of doubles for Fe_3O_4@C@PtPd nanocomposites locate at Pt 4f7/2 (71.38 eV), Pt 4f5/2 (74.81 eV), and Pt 4f7/2 (72.29 eV), Pt 4f5/2 (76.39 eV), which are assigned to Pt^0 and Pt^{II} species, respectively.[50−52] In the curve fitting Pd 3d spectrum (Figure 4B), a small quantity of Pd(II) species were still found, which is probably due to the adsorption of Pd(II) on the CMNPs making the complete reduction of Pd(II) diffcult to achieve.

The C1s electronic states for the CMNPs, Fe_3O_4@C@Pt and Fe_3O_4@C@PtPd nanocomposites are observed at 282.2, 282.7, and 284.8 eV, respectively, and 69.2 eV for Pt 4f7/2 in Pt^0 species of Fe_3O_4@C@Pt nanocomposties, which is much lower than the binding energy of Pt 4f7/2 (E_b = 70.61−71.30 eV) for Pt^0 species.[53−55] The increase and decrease in binding energy of C1s and Pt 4f characteristic peaks after in situ loading Pt and Pd on the CMNPs indicates there is an interaction between the outer-shell electrons of C and Pt nanoparticles that leads to a small change in electron density of C and Pt, which in turn causes some contributions toward small core level shifts for these atoms. The binding energy of Pt 4f was further changed from 69.20 eV to 71.38 eV after the introduction of Pd, as shown in Figure 4A. In Figure 4B, the binding energy of Pd3d in Fe_3O_4@C@PtPd nanocomposites is 335.64 eV; however, 335.10 and 335.80 eV for Pd3d in Pd^0 species were reported by Sarapatka et al.,[56−58] slightly higher than the binding energy of Pd3d in Pd/Pt bimetals (E_b = 335.00-335.40 eV).[59] The change in binding energy of C1s and the shift of Pt 4f for the supported Pt nanoparticles compared to that for PtPd nanoalloys suggests the presence of chemical shifts which depends on the polarization of electron bond between nearest neighbor atoms. This result indicates that the electronic coupling between Pt and C & Pd has been achieved. The electronic coupling can result in shifts for the d-band center position of the catalysts which plays a decisive role in determining the catalytic performance because the position of the d-band center is directly related to the adsorption energies

of the reactants on a catalyst as well as their activation barriers.[60,61]

3.2. Catalytic Properties of the Supported Pt−Pd Nanoalloys. The catalytic property of the Fe_3O_4@C@PtPd nanocatalysts was quantitatively evaluated with the catalytic reduction of 4-NP into 4-AP by $NaBH_4$ in water as a model system. The reduction kinetics was monitored by UV-vis absorption spectroscopy of the reaction mixture. 4-NP showed a distinct spectral profile with an absorption maximum at 317 nm in water, and the absorption peak of 4-NP shifted to 400 nm when $NaBH_4$ was added because of the formation of the *p*-nitrophenolate ion under alkaline condition.[62,63] So the reduction kinetics was easily recorded by monitoring the decrease in absorbance of the reaction mixture with the increase in reaction time after adding catalysts.

Initially, as a control experiment, the catalytic ability of CMNPs in the absence of noble metals was examined. The color (yellow) of the reaction mixture remained unaltered when the reaction mixture was kept statically for one month. It's indicated that the supports did not show catalytic activity. In the presence of colloidal dispersion of Fe_3O_4@C@PtPd catalysts, the bright yellow solution quickly faded, as shown in Figure S4 in the Supporting Information. The application of spectrophotometer revealed that the absorption of 4-NP at 400 nm decreases along with a concomitant increase of the ~298 nm peak of 4-AP. As shown in Figure 5a, a new peak appeared at around 298 nm and gradually increased as the reaction proceeds, revealing the reduction of 4-NP to 4-AP, which indicated the catalysts catalyzed reduction of 4-NP rather than merely adsorbing it onto the nanocomposites in spite of the great adsorption abilities of CMNPs, but this is an important factor in possessing the high catalytic activity. The UV-vis spectra in the Figure 5a showed an isosbestic point at around 318 nm, suggesting that the catalytic reduction of 4-NP generates 4-AP only without by-products.[64] From the spectrogram, a slight drop of the black curve in comparison to other curves at the level of around 500 nm can be observed. This is because the addition of catalysts leads to the increase in absorbance of the mixed solution in the full spectrum.

According to the previous reports, there is always an "induction time" before reduction of 4-NP in the reaction as a result of adsorption of 4-NP onto the surface of the catalysts and the reaction of the dissolved oxygen with $NaBH_4$ prior to the reduction of 4-NP by $NaBH_4$.[65,66] In Figure 5b, a very short induction time less than 13 s was barely recorded and the correlation of ln(At/A0) versus time keep linear during the recording time (inset). We tend to attribute the very short induction time to the enhanced ultrahigh catalytic activity of the supported Pt−Pd alloy by means of synergistic effects between the nanoalloys and supports. Of course, the strong dispersibility in reaction solution and high charged surface of CMNPs are important factors in shortening the induction time as well.

To ensure the reduction rate is independent of the concentration of $NaBH_4$, the effect of the concentration of $NaBH_4$ on the apparent first-order rate constant was investigated and was shown in Figure S5 in the Supporting Information. It can be observed that the apparent rate constant increased with increasing concentration of $NaBH_4$ and then the reaction rate is independent of $NaBH_4$ concentration at a certain level. In the experiments, we used excess $NaBH_4$ to ensure that the catalytic reduction of 4-NP is zero-order with respect to concentration of $NaBH_4$ and follows first-order rate law with respect to 4-NP concentration.

The enhanced activity of the supported Pt−Pd nanolloys was compared with the supported monometallic nanocatalysts and bimetallic nanocatalyts synthesized via the co-reduction route. The monometallic Pd nanocatalysts supported on CMNPs (simplified as S_{Pd}) were prepared via approach of preparing S_{Pt} samples and the bimetallic Pt−Pd nanocatalyts supported on CMNPs at 25 and 60 °C via the co-reduction route with the same ethanol reduction with the preparation of S_{Pt} sample is simplified as S_{25} and S_{60}, respectively. For comparison, the amount of noble metal in all samples are controlled to be equal to the corresponding amount about 90 nmol in the experiment of reduction of 4-NP.

As shown in Figure 6, it can be visually observed good linear correlations of ln (C_t/C_0) versus time for all samples. Then, the

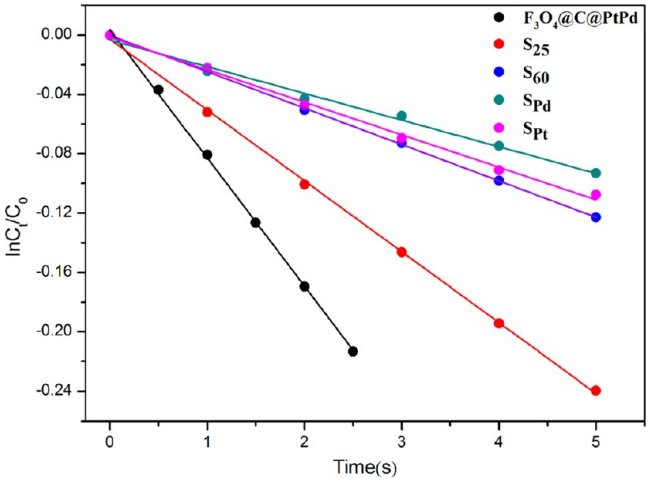

Figure 6. Plots of ln (C_t/C_o) of 4-NP versus reaction time for all kinds of compared nanocomposites. ([4-NP] = 5.0×10^{-5} mol/L; [$NaBH_4$] = 2.0×10^{-3} mol/L; [PtPd] = 18×10^{-6} mol/L).

apparent rate constants obtained from the slopes of the linearly fitted plots are 86.3×10^{-3}, 47.7×10^{-3}, 24.5×10^{-3} , $21.9.0 \times 10^{-3}$and 18.0×10^{-3} S^{-1} for the F_3O_4@C@PtPd, S_{25}, S_{60}, S_{Pt}, and S_{Pd} samples, respectively. The k_{app} values show that the catalytic activity of supported Pt−Pd nanocatalysts via two-step in situ synthesis method is superior to that of supported Pt−Pd bimetallic nanocatalysts via co-reduction method, and the enhanced catalytic activity is about 4 times higher than that of the supported monometallic counterparts on the basis of the amount of monometals is the same, which is 90 nmol. The results demonstrated the catalytic performance of bimetallic nanocatalysts is really enhanced by alloying of two monometallic counterparts. However, our result is different from the reports by Zhang and Seong et al., their Pd−Pt nanoalloys were all prepared by co-reduction.[36,67] They found that the catalytic efficiency of Pd−Pt nanoalloys is inferior to the Pd nanoparticles and has a relationship of linear increase with Pd percentage for the catalytic reduction of 4-NP by $NaBH_4$. In other words, Pd dominates the catalytic activities of Pd−Pt bimetals in their experiment and bimetallic nanocatalysts do not exhibit the superiority of the alloy catalysts, which makes no difference between their Pd−Pt nanoalloys and two kinds of monometals independent on the supports. The reason why our results are different to our reports are employ of co-reduction which results in the generation of poorly defined structures.

Further investigation of catalytic property of the supported nanoalloys includes alloy-composition-dependent catalytic activity. We could tune catalytic property of the supported nanoalloys and obtain optimum catalytic property by changing the composition of the supported nanoalloys. In the experiment, different Pd/Pt ratios were obtained by changing the volume of added $PdCl_2$ and fixing volume of K_2PtCl_4. Pd and Pt content of the samples were analyzed by means of the ICP spectrometer and were shown in the Table 1. The well-linear relation between $\ln(C_t/C_0)$ and reaction time is observed for all samples catalyzing the reduction of 4-NP in Figure 7 and the apparent rate constants which were estimated from first-order reaction kinetics were summarized in Table 1. We could obviously get the conclusion that the supported nanoalloys with a 2.07:1 ratio of Pd to Pt show the optimum catalytic activity with the highest normalized rate constant about 12.03 $nmol^{-1}$ $s^{-1}$and the catalytic activity of the supported nanoalloys does not exhibit an increase relationship with Pd percentage from the Table 1. Furthermore, we compared it with that of Pd-based nanocatalysts reported previously listed in Table S1 in the Supporting Information and find the molar specific activity of the supported Pt−Pd nanoalloys in our experiments is much higher than that of most reports for the catalytic reduction of p-NP by $NaBH_4$ except the result from Zhang et al. in entry 6 of Table S1 in the Supporting Information. A minute quantity of Pd/Pt nanoalloys, as much as approximately 6−8 orders of magnitude lower than that of other results, was used and high apparent rate constants were obtained in his experiments.

Table 1. Summary of the Composition Effect of the Supported Nanoalloys on the Activity Parameter *k* for the Catalytic Reduction of 4-NP by $NaBH_4$

sample name	Pt (ug)	Pd (ug)	k_{app} [a] (s^{-1})	Pd/Pt (mol)	k_{nor} [b] ($nmol^{-1}$ s^{-1})
S_1	112.9	35.6	3.6	0.58	3.94
S_2	108.8	75.2	8.3	1.27	6.56
S_3	106.7	120.4	20.2	2.07	12.03
S_4	100.4	161.5	16.1	2.95	7.92
S_5	97.4	232.2	10.8	4.37	4.03

[a] k_{app} = apparent rate constant. [b] k_{nor} = normalized rate constant with respect to the total amount of Pt and Pd.

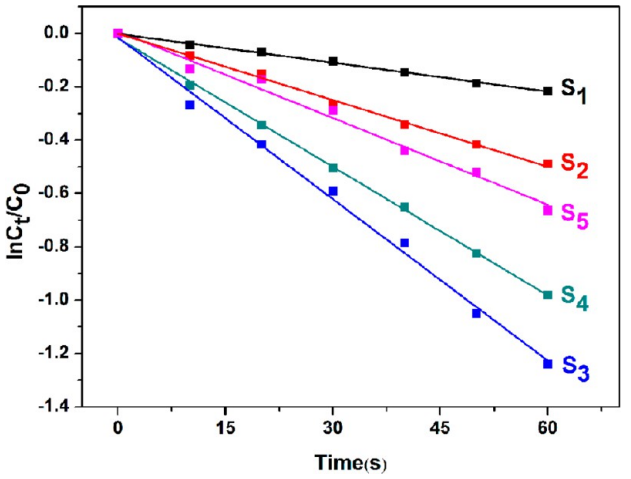

Figure 7. Plots of $\ln(C_t/C_o)$ of 4-NP versus reaction time for different composites of F_3O_4@C@PtPd nanocatalysts at $[NaBH_4] = 5.0 \times 10^{-2}$ mol/L, $[4\text{-NP}] = 5.0 \times 10^{-5}$ mol/L, and to this reaction solution, 50 uL (0.05%) of aqueous solution of nanocatalysts with different composites was added.

The results in our experiments illustrate that the catalytic activity of bimetallic nanocatalysts could be enhanced by alloying of two monometallic counterparts and supporting on an appropriate support. We attribute it to the excellent synergistic effect due to the modification of the electronic structure of Pt−Pd nanoalloys via partial electron transfer from CMNPs to Pt at the nanoscale interface, which improves adsorption and activation of *p*-nitrophenolate ions on the surface of nanoalloys.

4. CONCLUSION

A facile two-step in situ synthesis method was successfully developed to prepare the well-defined Pt−Pd nanoalloys supported on F_3O_4@C. The alloy structure of the supported Pt−Pd bimetallic nanoparticles was affirmed unambiguously by EDS line scanning. The as-prepared F_3O_4@C@PtPd nanocatalysts exhibited an excellent activity for catalytic reduction of 4-NP compared to the supported Pt−Pd bimetallic nanocomposites by co-reduction and Pd-based nanocatalysts reported previously. We attribute it to the excellent synergistic effect and the well-defined structure of nanoalloys by the method of in situ synthesis. The supported nanoalloys produced via the in-situ synthesis enhanced the synergistic effect remarkably. Besides, this method can also be used to prepare the supported nanoalloys that are obtained with difficulties by the common co-reduction method. Hence, the two-step in situ synthesis method of preparing supported nanoalloys is significant in designing high-performance catalysts in terms of activity and stability.

■ ASSOCIATED CONTENT

Supporting Information

XRD patterns of different samples, TEM figure and XPS survey spectrum of as-prepared samples in the each of step of synthesis, color changes for mixture solution after the addition of the catalyst, plots of the apparent rate constant vs the concentration of $NaBH_4$, the summary table of catalytic activity of nanomaterials for the catalytic reduction. This material is available free of charge via the Internet at http://pubs.acs.org.

■ AUTHOR INFORMATION

Corresponding Authors

*E-mail: liren@ustc.edu.cn (R.L.).
*E-mail: cqw@ustc.edu.cn (Q.C.).

Notes

The authors declare no competing financial interest.

■ ACKNOWLEDGMENTS

This work was supported by the National Natural Science Foundation (NSFC, 21071137).

■ REFERENCES

(1) Sharma, M. K.; Buchner, R. D.; Scharmach, W. J.; Papavassiliou, V.; Swihart, M. T. *Aerosol Sci. Technol.* **2013**, *47*, 858−866.
(2) Maharana, P. K.; Bharadwaj, S.; Jha, R. *J. Appl. Phys.* **2013**, *114*, 014304 (4 pp.)−014304 (4 pp.).
(3) Banin, U. *Nat. Mater.* **2007**, *6*, 625−626.
(4) Hong, J. W.; Kim, D.; Lee, Y. W.; Kim, M.; Kang, S. W.; Han, S. W. *Angew. Chem., Int. Ed.* **2011**, *50*, 8876−8880.

(5) Kang, Y.; Qi, L.; Li, M.; Diaz, R. E.; Su, D.; Adzic, R. R.; Stach, E.; Li, J.; Murray, C. B. *Acs Nano* **2012**, *6*, 2818−2825.
(6) Ferrando, R.; Jellinek, J.; Johnston, R. L. *Chem. Rev.* **2008**, *108*, 845−910.
(7) Radillo-Diaz, A.; Coronado, Y.; Perez, L. A.; Garzon, I. L. *Eur. Phys. J. D* **2009**, *52*, 127−130.
(8) Bernardotto, G.; Menegazzo, F.; Pinna, F.; Signoretto, M.; Cruciani, G.; Strukul, G. *Appl. Catal., A* **2009**, *358*, 129−135.
(9) Wang, W.; Huang, Q.; Liu, J.; Zou, Z.; Li, Z.; Yang, H. *Electrochem. Commun.* **2008**, *10*, 1396−1399.
(10) Armbruester, M.; Kovnir, K.; Friedrich, M.; Teschner, D.; Wowsnick, G.; Hahne, M.; Gille, P.; Szentmiklosi, L.; Feuerbacher, M.; Heggen, M.; Girgsdies, F.; Rosenthal, D.; Schloegl, R.; Grin, Y. *Nat. Mater.* **2012**, *11*, 690−693.
(11) Son, S. U.; Jang, Y.; Park, J.; Na, H. B.; Park, H. M.; Yun, H. J.; Lee, J.; Hyeon, T. *J. Am. Chem. Soc.* **2004**, *126*, 5026−5027.
(12) Studt, F.; Abild-Pedersen, F.; Bligaard, T.; Sorensen, R. Z.; Christensen, C. H.; Norskov, J. K. *Science* **2008**, *320*, 1320−1322.
(13) Yang, B.; Burch, R.; Hardacre, C.; Headdock, G.; Hu, P. *ACS Catal.s* **2012**, *2*, 1027−1032.
(14) Wang, X.-M.; Wang, M.-E.; Zhou, D.-D.; Xia, Y.-Y. *Phys. Chem. Chem. Phys.* **2011**, *13*, 13594−13597.
(15) Alonso, D. M.; Wettstein, S. G.; Dumesic, J. A. *Chem. Soc. Rev.* **2012**, *41*, 8075−8098.
(16) Sankar, M.; Dimitratos, N.; Miedziak, P. J.; Wells, P. P.; Kiely, C. J.; Hutchings, G. J. *Chem. Soc. Rev.* **2012**, *41*, 8099−8139.
(17) Li, X.; Park, S.; Popov, B. N. *J. Power Sources* **2010**, *195*, 445−452.
(18) Jiang, H.-L.; Akita, T.; Ishida, T.; Haruta, M.; Xu, Q. *J. Am. Chem. Soc.* **2011**, *133*, 1304−1306.
(19) Edwards, J. K.; Ntainjua, N. E.; Carley, A. F.; Herzing, A. A.; Kiely, C. J.; Hutchings, G. J. *Angew. Chem., Int. Ed.* **2009**, *48*, 8512−8515.
(20) Kugai, J.; Miller, J. T.; Guo, N.; Song, C. *J. Catal.* **2011**, *277*, 46−53.
(21) Liu, X.; Wang, A.; Zhang, T.; Su, D.-S.; Mou, C.-Y. *Catal. Today* **2011**, *160*, 103−108.
(22) Jiang, K.; Zhang, H.-X.; Yang, Y.-Y.; Mothes, R.; Lang, H.; Cai, W.-B. *Chem. Commun.* **2011**, *47*, 11924−11926.
(23) Mallick, K.; Witcomb, M. J.; Scurrell, M. S. *Appl. Catal., A* **2004**, *259*, 163−168.
(24) Chu, K. J.; Shan, C.; Soares, J. B.; Penlidis, A. *Macromol. Chem. Phys.* **1999**, *200*, 2372−2376.
(25) An, Q.; Yu, M.; Zhang, Y.; Ma, W.; Guo, J.; Wang, C. *J. Phys. Chem. C* **2012**, *116*, 22432−22440.
(26) Kaiser, J.; Leppert, L.; Welz, H.; Polzer, F.; Wunder, S.; Wanderka, N.; Albrecht, M.; Lunkenbein, T.; Breu, J.; Kuemmel, S.; Lu, Y.; Ballauff, M. *Phys. Chem. Chem. Phys.* **2012**, *14*, 6487−6495.
(27) Chassagneux, F.; Bois, L.; Simon, J.-P.; Desroches, C.; Brioude, A. *J. Mater. Chem.* **2011**, *21*, 11947−11955.
(28) Hosseinkhani, B.; Sobjerg, L. S.; Rotaru, A.-E.; Emtiazi, G.; Skrydstrup, T.; Meyer, R. L. *Biotechnol. Bioeng.* **2012**, *109*, 45−52.
(29) Jin, Z.; Xiao, M.; Bao, Z.; Wang, P.; Wang, J. *Angew. Chem., Int. Ed.* **2012**, *51*, 6406−6410.
(30) Chen, R.; Jiang, Y.; Xing, W.; Jin, W. *Ind. Eng. Chem. Res.* **2013**, *52*, 5002−5008.
(31) Madhavan, N.; Jones, C. W.; Weck, M. *Acc. Chem. Res.* **2008**, *41*, 1153−1165.
(32) Wang, H.; Li, Y.; Luo, Z.; Zhou, S.; Sheng, J.; Chen, Q. *Nano* **2010**, *5*, 333−339.
(33) Hu, H.; Chen, Q.-W.; Wang, H.; Li, R.; Zhong, W. *J. Mater. Chem.* **2011**, *21*, 13062−13067.
(34) Li, R.; Zhang, P.; Huang, Y.; Zhang, P.; Zhong, H.; Chen, Q. *J. Mater. Chem.* **2012**, *22*, 22750−22755.
(35) Sun, X.; Guo, S.; Liu, Y.; Sun, S. *Nano Lett.* **2012**, *12*, 4859−4863.
(36) Zhang, K.; Hu, X.; Liu, J.; Yin, J.-J.; Hou, S.; Wen, T.; He, W.; Ji, Y.; Guo, Y.; Wang, Q.; Wu, X. *Langmuir* **2011**, *27*, 2796−2803.
(37) You, H.; Yang, S.; Ding, B.; Yang, H. *Chem. Soc. Rev.* **2013**, *42*, 2880−2904.
(38) Kundu, P.; Nethravathi, C.; Deshpande, P. A.; Rajamathi, M.; Madras, G.; Ravishankar, N. *Chem. Mater.* **2011**, *23*, 2772−2780.
(39) Li, W.; Kuai, L.; Qin, Q.; Geng, B. *J. Mater. Chem. A* **2013**, *1*, 7111−7117.
(40) Wang, H.; Sun, Y.-B.; Chen, Q.-W.; Yu, Y.-F.; Cheng, K. *Dalton Trans.* **2010**, *39*, 9565−9569.
(41) Li, R.; Zhang, H.; Chen, Q.-W.; Yan, N.; Wang, H. *Analyst* **2011**, *136*, 2527−2532.
(42) Lee, W. R.; Kim, M. G.; Choi, J. R.; Park, J. I.; Ko, S. J.; Oh, S. J.; Cheon, J. *J. Am. Chem. Soc.* **2005**, *127*, 16090−16097.
(43) Zhang, H.; Jin, M.; Wang, J.; Li, W.; Camargo, P. H. C.; Kim, M. J.; Yang, D.; Xie, Z.; Xia, Y. *J. Am. Chem. Soc.* **2011**, *133*, 6078−6089.
(44) Bard, A. J.; Faulkner, L. R. *Electrochemical Methods: Fundamentals and Applications*, 2nd ed.; Wiley: New York, 2001.
(45) Wang, X.; Zhuang, J.; Peng, Q.; Li, Y. D. *Nature* **2005**, *437*, 121−124.
(46) Wang, D.; Li, Y. *Adv. Mater.* **2011**, *23*, 1044−1060.
(47) Peng, Z.; Yang, H. *Nano Today* **2009**, *4*, 143−164.
(48) Zhang, Q.; Lee, J. Y.; Yang, J.; Boothroyd, C.; Zhang, J. *Nanotechnology* 2007, *18*.
(49) Wang, C.; Peng, S.; Chan, R.; Sun, S. *Small* **2009**, *5*, 567−570.
(50) Hsin, Y. L.; Hwang, K. C.; Yeh, C.-T. *J. Am. Chem. Soc.* **2007**, *129*, 9999−10010.
(51) He, Y.-B.; Li, G.-R.; Wang, Z.-L.; Ou, Y.-N.; Tong, Y.-X. *J. Phys. Chem. C* **2010**, *114*, 19175−19181.
(52) Prabhuram, J.; Zhao, T. S.; Wong, C. W.; Guo, J. W. *J. Power Sources* **2004**, *134*, 1−6.
(53) Battistoni, C.; Giuliani, A. M.; Paparazzo, E.; Tarli, F. *J. Chem. Soc., Dalton Trans.* **1984**, 1293−1299.
(54) Legare, P.; Lindauer, G.; Hilaire, L.; Maire, G.; Ehrhardt, J. J.; Jupille, J.; Cassuto, A.; Guillot, C.; Lecante, J. *Surf. Sci.* **1988**, *198*, 69−78.
(55) Thiele, J.; Barrett, N. T.; Belkhou, R.; Guillot, C.; Koundi, H. *J. Phys.: Condens. Matter* **1994**, *6*, 5025−5038.
(56) Kohiki, S.; Hamada, T. *J. Mater. Sci.* **1990**, *25*, 1344−1346.
(57) Sarapatka, T. J. *J. Phys. Chem.* **1993**, *97*, 11274−11277.
(58) Tressaud, A.; Khairoun, S.; Touhara, H.; Watanabe, N. *Z. Anorg. Allg. Chem.* **1986**, *541*, 291−299.
(59) Han, M.; Mrozek, P.; Wieckowski, A. *Phys. Rev. B* **1993**, *48*, 8329−8335.
(60) Norskov, J. K.; Abild-Pedersen, F.; Studt, F.; Bligaard, T. *Proc. Nat. Acad. Sci. U.S.A.* **2011**, *108*, 937−943.
(61) Hammer, B.; Norskov, J. K. In *Advances in Catalysis, Vol. 45: Impact of Surface Science on Catalysis*; Gates, B. C., Knozinger, H., Eds.; Academic Press: San Diego, 2000; Vol. *45*, pp 71−129.
(62) Ghosh, S. K.; Mandal, M.; Kundu, S.; Nath, S.; Pal, T. *Appl. Catal., A* **2004**, *268*, 61−66.
(63) Murugadoss, A.; Chattopadhyay, A. *Nanotechnology* **2008**, *19*, No. 015603.
(64) Deng, Y.; Cai, Y.; Sun, Z.; Liu, J.; Liu, C.; Wei, J.; Li, W.; Liu, C.; Wang, Y.; Zhao, D. *J. Am. Chem. Soc.* **2010**, *132*, 8466−8473.
(65) Zeng, J.; Zhang, Q.; Chen, J.; Xia, Y. *Nano Lett.* **2010**, *10*, 30−35.
(66) Signori, A. M.; Santos, K. d. O.; Eising, R.; Albuquerque, B. L.; Giacomelli, F. C.; Domingos, J. B. *Langmuir* **2010**, *26*, 17772−17779.
(67) Oh, S.-D.; Kim, M.-R.; Choi, S.-H.; Chun, J.-H.; Lee, K.-P.; Gopalan, A.; Hwang, C.-G.; Sang-Ho, K.; Hoon, O. J. *J. Ind. Eng. Chem.* **2008**, *14*, 687−692.